A Practical Method of BLDCM Based on High-precision Estimation of the Rotor Position

ZHOU Aiguo, YANG Lang, PAN Qiangbiao, and SHEN Yong

***Abstract*—Approaches of staring sensorless BLDCM have been of the research concentrations in the last decade. This paper in the first place elaborates connections between winding inductance and rotor position as well as relationships between torque and torque angle. Based on theories above, a new method of estimating the rotor position and starting sensorless BLDCM is proposed. This method uses voltage pulses, which are generated in two-phase and three-phase conduction modes, to identify the rotor position within a maximum error of ± 7.5 in electrical degrees. In this way, starting vibration will be reduced, leading to a higher starting success rate. Experiments on a sample BLDCM prove the feasibility of this new method.**

***Index Terms*—BLDCM, inductance, initial position, sensorless**

I. Introduction

SENSORLESS Brushless Direct Current Motors (BLDCM) have been popular in various industrial applications in the recent ten years, especially in pumps, for its high reliability, small size and light weight [1]-[2]. A traditional way of rotor position detection based on BEMF ZCP (Back Electromotive Force zero-crossing point) has been widely applied in sensorless BLDCM. However, BEMF ZCP cannot be detected when no rotor movement causes BEMF signals [3].

Nevertheless, estimation of initial rotor position must be executed, otherwise vibration or reversal may occur during the starting period.

References [4]-[6] can estimate the initial rotor position within a maximum error of ± 15 in electrical degrees. However in this paper, the estimation error of rotor position will be narrowed down to ± 7.5 in electrical degrees and a specific starting-up method follows up. Moreover, principles of estimation based on inductance variation are elaborated in details.

II. Analysis of Winding Inductance

In A-B-C coordinate frame, three-phase voltages can be expressed as

$$[u_A\, u_B\, u_C]^T = \begin{bmatrix} R & 0 & 0 \\ 0 & R & 0 \\ 0 & 0 & R \end{bmatrix} \bullet [i_A\, i_B\, i_C]^T + p \begin{bmatrix} \psi_A(\theta, i) \\ \psi_B(\theta, i) \\ \psi_C(\theta, i) \end{bmatrix} \quad (1)$$

where u_A , u_B and u_C are voltages; R is the resistance; i_A , i_B and i_C are currents; $\psi_A(\theta, i)$, $\psi_B(\theta, i)$ and $\psi_C(\theta, i)$ are total flux linkage of phase A, B and C respectively. p is differential operator and θ is the angle between rotor's d-axis and α-axis in α-β coordinate frame.

According to (1), as long as the phase voltage remains constant, the current response is only affected by total flux linkage which contains the rotor position information. Actually, total flux linkage depends on winding inductance, that is, rotor position information lies in winding inductance.

Winding inductance comprises of two parts - leakage inductance (ignored) and main inductance. Under the effect of both magnetomotive force (MMF) and permanent magnet flux (PM flux), main inductance varies in accordance with the rotor position [4].

A. The Effect of MMF

The main inductance of phase winding can be generally expressed as

$$L_A \propto N_A^2 \bullet \Lambda_m \quad (2)$$

where N_A is the equivalent turns of windings and Λ_m is the permeance of the main inductance. Reluctance is the reciprocal of permeance, that is $R_m = 1/\Lambda_m$. According to (2), L_A is proportional to Λ_m when winding distribution patterns and winding turns are ascertained.

Magnetic circuit in BLDCM passes through the air gap, PM and the rotor core. The total reluctance can be described as below.

$$\begin{aligned} R_m &= R_{m0} + R_{mPM} + R_{mFe} \\ &= \frac{l_0}{\mu_0 A_0} + \frac{l_{PM}}{\mu_{PM} A_{PM}} + \frac{l_{Fe}}{\mu_{Fe} A_{Fe}} \end{aligned} \quad (3)$$

where l_0 , l_{PM} and l_{Fe} are length of magnetic circuit path; μ_0 , μ_{PM} and μ_{Fe} are permeability; A_0 , A_{PM} and A_{Fe} are sectional areas of air, PM and the rotor core respectively.

Fig. 1a, Fig. 1b and Fig. 1c show three kinds of equivalent magnetic circuits with different rotor positions. μ_{Fe} is much larger than μ_{PM} which nearly equals μ_0 , as a result, the longer l_{PM} is, the larger R_m is [3]. In the situation of Fig. 1a, stator current flows into phase A and out of phase B, creating MMF F_a which is parallel to PM axis. So l_{PM} maximizes while l_{Fe} minimizes. Based on (3), R_m maximizes and inductance minimizes. In the situation of Fig. 1b,

Manuscript is received on October 15, 2015; revised on February 5, 2016.

ZHOU Aiguo is an associate professor in School of Mechanical and Energy Eng., Tongji University, China, e-mail: zhouaiguo@tongji.edu.cn.

YANG Lang is a postgraduate student in School of Mechanical and Energy Eng., Tongji University, China, e-mail: 626387522@qq.com.

PAN Qiangbiao is a postgraduate student in School of Mechanical and Energy Eng., Tongji University, China, e-mail: 149679087 @qq.com.

SHEN Yong is a professor in School of Automotive Studies, Tongji University, China, e-mail: shenyong@tongji.edu.cn.

MMF remains the same but PM axis is 60° away from F_a. l_{PM} becomes smaller while l_{Fe} becomes larger. So inductance gets larger. In the situation of Fig. 1c, PM axis is perpendicular to F_a and inductance maximizes.

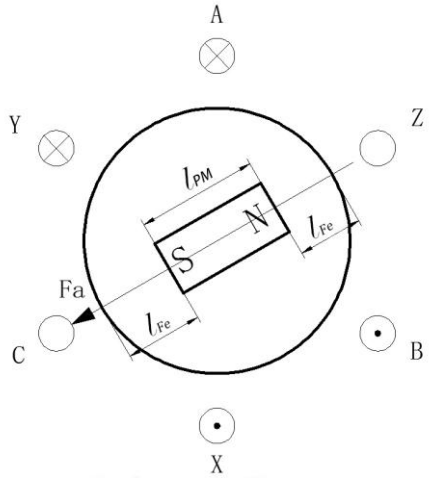

Fig. 1a. Rotor axis which is parallel to F_a

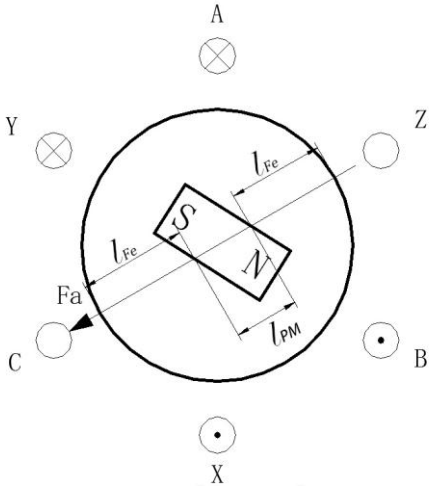

Fig. 1b. Rotor axis which is 60° away from F_a

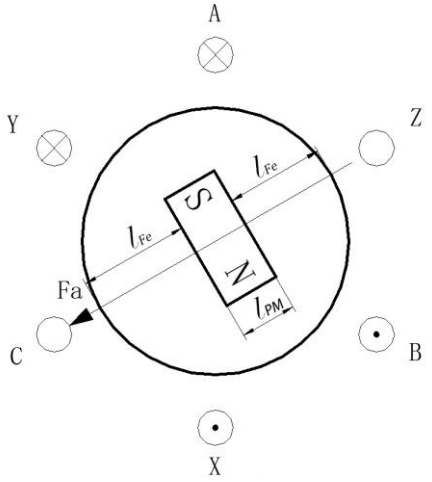

Fig. 1c. Rotor axis which is perpendicular to F_a

B. The Effect of PM flux

PM flux is strong enough to influence the magnetic situation of stator windings. Keep winding current equal zero (no effect of MMF), PM flux interlinks the most with phase A when PM axis is parallel to phase A axis. At this time, winding A is greatly magnetized hence inductance minimizes. PM flux interlinks the least with phase A when PM axis is perpendicular to phase A axis. Then winding A is less magnetized hence inductance maximizes [5] [10]. The relationship between winding inductance and rotor position can be roughly expressed in Fig. 3.

Above all, effects on inductance by PM flux and MMF are synchronous.

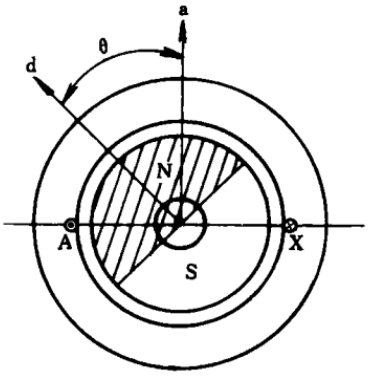

Fig. 2. Schematic diagram of the structure of PMSM

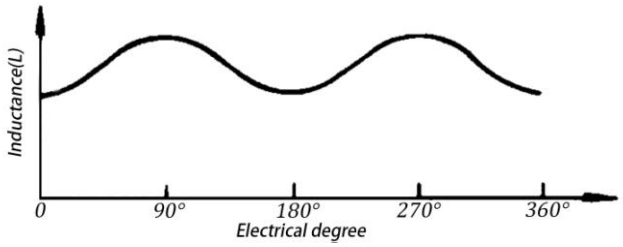

Fig. 3. Relationship between inductance and rotor position

In two-phase conduction mode, six different MMFs of the constant amplitude are generated by stator windings. Considering effects of MMF and PM flux respectively, because every two MMFs are 60° away from each other, inductance under two opposite MMFs are the same [6]. That is $L_2=L_5> L_1=L_4> L_3=L_6$.

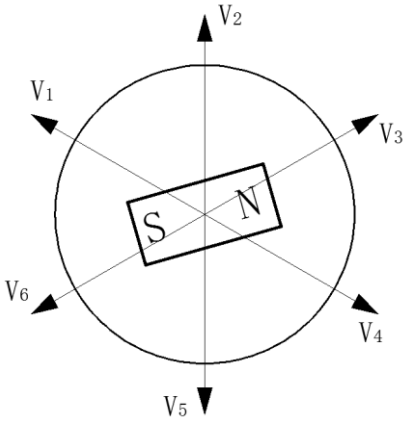

Fig. 4. Six MMFs generated by stator windings

C. The Effect of MMF Combined with PM Flux

MMF and PM flux acting together for enough time will induce armature reaction which further changes the stator magnetic situation. If the angle between MMF and PM north pole is less than 90°, MMF will magnetize PM. Otherwise, it will degauss PM. According to magnetizing curve, PM is easy to degauss but hard to magnetize. Such as in Fig. 4, V_3 and V_6 are equal in amplitude but opposite in direction. V_6 degausses PM so that the magnetic circuit becomes less saturated and inductance increases. V_3 magnetizes the PM so that the saturation of the magnetic circuit keeps alike and inductance remains unchanged.

III. Relationship Between Torque Angle and Output Torque

BLDCM has a square-wave air gap flux. In view that the magnet in the machine has an arc of 2β, its flux density will have a constant magnitude of B_m over 2β in the positive half cycle and $-B_m$ over 2β in the negative half cycle as shown in Fig. 5.

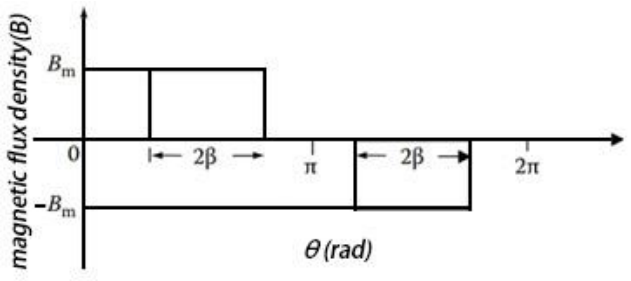

Fig. 5. Air gap flux density for BLDCM

According to [11], its fundamental wave, which is a sinusoid wave will have a peak, B_{m1}, obtained by using Fourier analysis as

$$B_{m1}=4/\pi B_m \sin\beta \tag{4}$$

The peak fundamental flux is given by

$$\varphi_{m1}=\frac{B_{m1}DL}{(p/2)}=\frac{8DL}{\pi P B_m \sin\beta} \tag{5}$$

where D is the inner diameter of the stator lamination, L is the effective length of the stator laminations assembled in a stack, and P is the number of pole-pairs.

The peak-induced BEMF is given by

$$E_m=2\pi f_s\left(T_{ph}k_\omega\right)\varphi_{m1}=\frac{4}{\pi}k_\omega T_{ph}DLB_m\omega_m\sin\beta \tag{6}$$

where k_ω is the factor of dimensions, T_{ph} is the turns of windings and ω_m is the mechanical angular velocity which can be obtained by dividing stator angular frequency by the number of pole-pairs. That is $\omega_m=2\pi f_s/P$.

The phase power is the product of the RMS induced EMF and conjugate of the RMS current given by

$$\begin{aligned}P&=\mathrm{Re}\left[3\left\{\frac{E_m(I_m)^*}{\sqrt{2}\sqrt{2}}\right\}\right]=\mathrm{Re}\left[\frac{3}{2}E_m\angle 90^\circ\bullet I_m\angle-\delta\right]\\&=\left(\frac{3}{2}\frac{4}{\pi}k_\omega T_{ph}DL\sin\beta\right)B_mI_m\omega_m\sin\delta\end{aligned} \tag{7}$$

where I_m is the amplitude of the phase current and δ is the angle by which the stator current exceeds rotor's magnetic field, which is called torque angle.

Then the torque can be written as

$$T_e=\frac{P}{\omega_m}\frac{3}{2}(DL)\left(\frac{4}{\pi}k_\omega T_{ph}I_m\right)(B_m\sin\beta)\sin\delta \tag{8}$$

Noticing that the effective turns of a sinusoidally distributed winding for the concentrated winding with T_{ph} can be written in the form of $4k_\omega T_{ph}/\pi$ and that can be termed as N_s turns per phase. In this case, the torque can be finally written as

$$T_e=\frac{3}{2}(DL)(N_sI_m)(B_m\sin\beta)\sin\delta \tag{9}$$

Once PMSM is produced, the diameter of the stator lamination, D, the effective length of the stator laminations, L, the effective turns of winding, N_s, magnitude, B_m, and the arc of the magnet, 2β have been ascertained. Therefore, controlling the magnitude of current, I_m, and torque angle, δ, can deliver specified torque at various speeds.

IV. Starting Methods Based on the Inductance Variation

The inductance variation law could be used to estimate the rotor position while the function of torque angle and output torque could be used to deliver a required torque.

A. Processes of Initial Rotor Position Estimation

Combining two-phase and three-phase conduction modes, windings can separately generate twelve MMFs as shown in Fig.6.

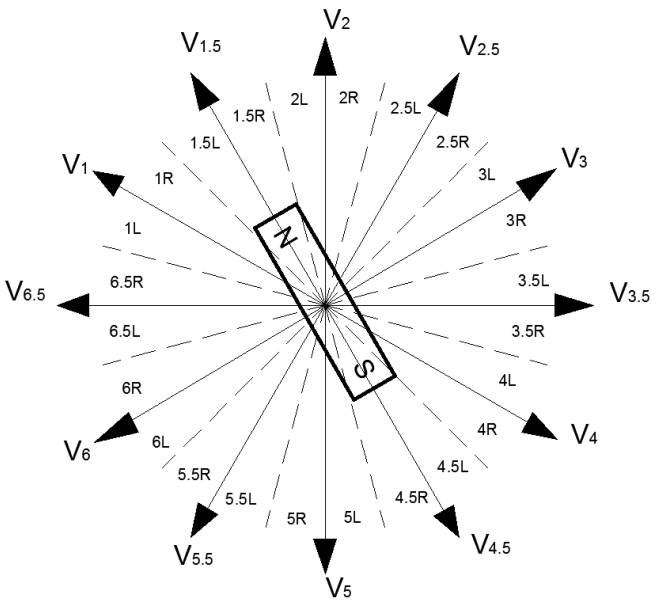

Fig. 6. Twelve MMFs generated by stator windings

V_1~V_6 are generated in two-phase conduction mode while $V_{1.5}$~$V_{6.5}$ are generated in three-phase conduction mode. The estimation methods include three processes.

Process one: Judge the rotor axis position. First set the amplitude of MMFs and duration time after which inject six short-time MMFs from V_1 to V_6 clockwise. Then sample the bus current at every commutating point and inject a zero vector immediately for the current falling to zero. The six

sampling current values present two kinds of regularity [9].

1). "Two large ones and four small ones" is presented if rotor axis lies closed to certain estimating MMF. With reference to Fig. 6, when rotor axis lies near V_2 and V_5 (in areas 2L~2R and 5L~5R), inductances under V_1, V_4 and V_3, V_6 are relatively large hence the sampling values are relatively small. Inductances under V_2 and V_5 are relatively small hence the sampling values are large.

2). "Four large ones and two small ones" is presented if the rotor axis lies in the middle of two adjacent estimating MMFs. With reference to Fig. 6, when the rotor axis lies in the middle of V_1 and V_2, V_4 and V_5 (in areas 1.5L~1.5R and 4.5L~4.5R), inductances under V_1,V_4 and V_2,V_5 are relatively small hence the sampling values are relatively large. Inductances under V_3 and V_6 are relatively large hence the sampling values are small.

Process two: Judge PM direction. Provided that north pole and south pole lie in areas 1.5L~1.5R and 4.5L~4.5R respectively, inject estimating MMF $V_{1.5}$ and $V_{4.5}$ successively for an adequate time to induce obvious armature reaction. $V_{1.5}$ magnetizes the PM so winding inductance stays alike while $V_{4.5}$ degausses PM so winding inductance drops. As a consequence, $I_{1.5}$ is larger than $I_{4.5}$.

Process three: Narrow down the estimation error. Assuming the north pole lies in area 1.5L~1.5R, inject V_1 and V_2 after which store I_1 and I_2. If $I_1 > I_2$, the north pole is in 1.5L otherwise in 1.5R. Process three minishes the error to $\pm 7.5^\circ$ or a maximum error of 15°.

The estimation processes can be concluded as Fig. 7.

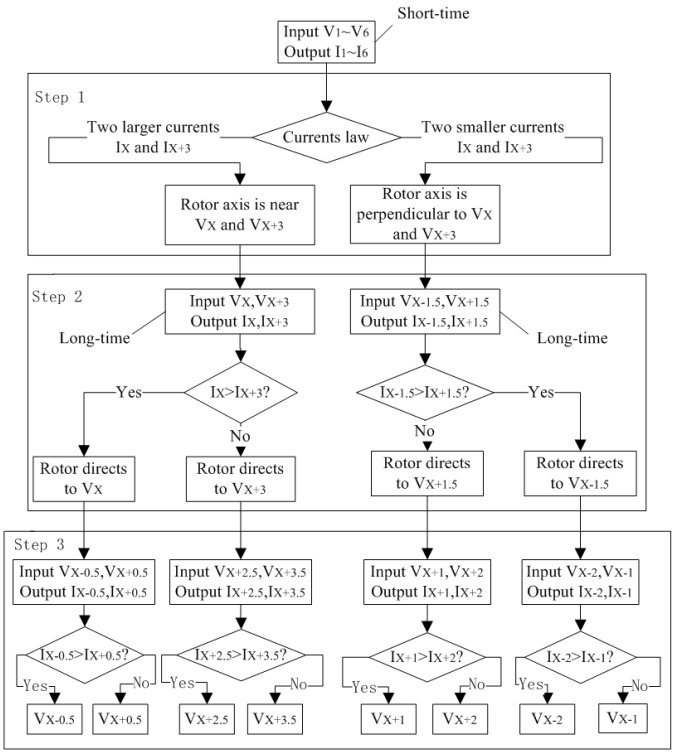

Fig. 7. The rotor position estimation flow chart

Duration of MMF in each process is worth discussing. In process one and three, duration should be as short as possible but the difference of sampling values should be distinguished. Overlong duration for a short-time pulse may induce armature reaction and a longer delay is additionally needed for the current dropping to zero. MMFs in process two last for longer to ensure armature reaction. Whereas the rotor won't easily be driven because the torque angle is not beyond 15°.

B. Selection of Driving MMF and PWM Duty

This paper adopts an open-loop control based on PWM. First identify the initial rotor position and then deploy a correlative driving MMF after setting a proper PWM duty. Once the rotor rotates at an adequate speed where BEMF ZCP can be detected by the detection circuit, the BEMF-based commutation mode begins and the starting procedure ends. This starting method is referred to the starting processes of BLDCM with hall sensors which also first creates a certain MMF and commutates when a new rotor position signal comes. It is worth noticing that BEMF ZCP could also be observed when estimating MMFs, V_1~V_6, are being injected one by one. It is because MMFs revolve around the rotor, in return, relatively, the rotor revolves around the windings.

According to (4), the torque angle should be 90° as much as possible to deliver a powerful torque. As shown in Fig. 6, assume the rotor rotates clockwise. When the north pole lies in area 1.5L, the driving MMF should be V_3. During the rotor rotates from 1.5L to 1.5R, $\sin\delta$ first increases and then drops. However, when the north pole is in 1.5R, the driving MMF should also be V_3 but $\sin\delta$ monotonously decreases. On the premise that the bus current keeps constant, the equivalent torque starting from 1.5L is bigger than that starting from 1.5R. To guarantee the starting torque steady, PWM_{START} duty when the rotor is in 1.5L should be marginally greater than that when the rotor is in 1.5R.

Moreover, a MMF produced in three-phase conduction mode can be regarded as a composition by two MMFs produced in two-phase conduction mode. Suppose the north pole is right at the position of V_2, $V_{3.5}$ is the driving MMFs. In this situation, $V_{3.5}$ could be regarded as a composition by V_3 and V_4. Assuming the phase current value is I_{ph}, the torque is given referring to (9) as follows

$$\begin{aligned} T_{3.5} &= T_3 + T_4 \\ &= \frac{3}{2}(DL)\left(N_s I_{ph}\right)\left(B_m \sin\beta\right)\bullet\left(\sin\left(\frac{\pi}{3}\right)+\sin\left(\frac{2\pi}{3}\right)\right) \\ &= \sqrt{3}\bullet\frac{3}{2}(DL)\left(N_s I_{ph}\right)\left(B_m \sin\beta\right) \end{aligned} \quad (10)$$

However, the torque in two-phase conduction mode is written as

$$T_{two} = \frac{3}{2}(DL)\left(N_s I_{ph}\right)\left(B_m \sin\beta\right) \quad (11)$$

Regardless of the energy loss of the inverter, $T_{3.5}$ is $\sqrt{3}$ times T_{two}. Therefore, PWM duty in three-phase conduction mode, $Duty_{three}$, should be set at $1/\sqrt{3}$ times PWM duty in two-phase conduction mode, $Duty_{two}$.

PWM_{START} duty configuration relies on the load, too. If the load is steady, the optimal duty can be acquired by trial and error. If the load is different each time the machine starts, the PWM duty could raise gradually until succeeding in starting. The starting flow chart is shown as Fig. 8.

TABLE I
ROTOR POSITION ESTIMATION METHODS AND CORRELATIVE DRIVING MMFS

Process one				Process Two			Process Three			Driving MMF	
Current Regularity	Short-time MMFs	Sampling Values	Rotor Axis Position	long-time MMFs	Sampling Values	North Pole Position	Short-time MMFs	Sampling Values	North Pole Position	MMF	PWM_{START} Duty
"Two large ones and four small ones"	V_1~V_6	Two large ones I_1,I_4	1L, 1R and 4L, 4R	V_1,V_4	$I_1>I_4$	1L, 1R	$V_{6.5}$, $V_{1.5}$	$I_{6.5}>I_{1.5}$	1L	$V_{2.5}$	$Duty_{threeL}$
								$I_{6.5}<I_{1.5}$	1R	$V_{2.5}$	$Duty_{threeR}$
					$I_1<I_4$	4L, 4R	$V_{3.5}$, $V_{4.5}$	$I_{3.5}>I_{4.5}$	4L	$V_{5.5}$	$Duty_{threeL}$
								$I_{3.5}<I_{4.5}$	4R	$V_{5.5}$	$Duty_{threeR}$
		Two large ones I_2,I_5	2L, 2R and 5L,5R	V_2,V_5	$I_2>I_5$	2L, 2R	$V_{1.5}$, $V_{2.5}$	$I_{1.5}>I_{2.5}$	2L	$V_{3.5}$	$Duty_{threeL}$
								$I_{1.5}<I_{2.5}$	2R	$V_{3.5}$	$Duty_{threeR}$
					$I_2<I_5$	5L, 5R	$V_{4.5}$, $V_{5.5}$	$I_{4.5}>I_{5.5}$	5L	$V_{6.5}$	$Duty_{threeL}$
								$I_{4.5}<I_{5.5}$	5R	$V_{6.5}$	$Duty_{threeR}$
		Two large ones I_3,I_6	3L, 3R and 6L, 6R	V_3,V_6	$I_3>I_6$	3L, 3R	$V_{2.5}$, $V_{3.5}$	$I_{2.5}>I_{3.5}$	3L	$V_{4.5}$	$Duty_{threeL}$
								$I_{2.5}<I_{3.5}$	3R	$V_{4.5}$	$Duty_{threeR}$
					$I_3<I_6$	6L, 6R	$V_{5.5}$, $V_{6.5}$	$I_{5.5}>I_{6.5}$	6L	$V_{1.5}$	$Duty_{threeL}$
								$I_{5.5}<I_{6.5}$	6R	$V_{1.5}$	$Duty_{threeR}$
"Four large ones and two small ones"	V_1~V_6	Two small ones I_1,I_4	2.5L, 2.5R and 5.5L, 5.5R	$V_{2.5}$, $V_{5.5}$	$I_{2.5}>I_{5.5}$	2.5L, 2.5R	V_2,V_3	$I_2>I_3$	2.5L	V_4	$Duty_{twoL}$
								$I_2<I_3$	2.5R	V_4	$Duty_{twoR}$
					$I_{2.5}<I_{5.5}$	5.5L, 5.5R	V_5,V_6	$I_5>I_6$	5.5L	V_1	$Duty_{twoL}$
								$I_5<I_6$	5.5R	V_1	$Duty_{twoR}$
		Two small ones I_2,I_5	3.5L, 3.5R and 6.5L, 6.5R	$V_{3.5}$, $V_{6.5}$	$I_{3.5}>I_{6.5}$	3.5L, 3.5R	V_3,V_4	$I_3>I_4$	3.5L	V_5	$Duty_{twoL}$
								$I_3<I_4$	3.5R	V_5	$Duty_{twoR}$
					$I_{3.5}<I_{6.5}$	6.5L, 6.5R	V_6,V_1	$I_6>I_1$	6.5L	V_2	$Duty_{twoL}$
								$I_6<I_1$	6.5R	V_2	$Duty_{twoR}$
		Two small ones I_3,I_6	1.5L, 1.5R and 4.5L, 4.5R	$V_{1.5}$, $V_{4.5}$	$I_{1.5}>I_{4.5}$	1.5L, 1.5R	V_1,V_2	$I_1>I_2$	1.5L	V_3	$Duty_{twoL}$
								$I_1<I_2$	1.5R	V_3	$Duty_{twoR}$
					$I_{1.5}<I_{4.5}$	4.5L, 4.5R	V_4,V_5	$I_4>I_5$	4.5L	V_6	$Duty_{twoL}$
								$I_4<I_5$	4.5R	V_6	$Duty_{twoR}$

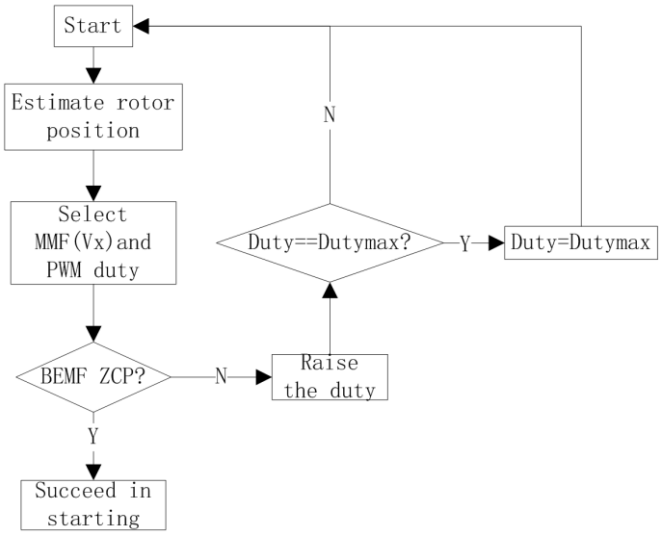

Fig. 8. The starting flow chart

Table I concludes estimation methods of the initial rotor position and the correlative driving MMFs. (Providing the rotor rotates clockwise.)

V. EXPERIMENTAL RESULTS

Methods mentioned above have been verified on a BLDC prototype (Fig. 9). BLDCM is supplied by a 15V DC power. PWM frequency is set at 20KHz with a duty of 50% and no load. Every MMF lasts for 1ms with a 1-ms interval and finally store the current value under every MMF. Fig. 10 is the current waveform displayed on the oscilloscope and Fig. 11 is the sampled current waveform depicted by 300 sample points. Fig. 10 and Fig. 11 present the "two large ones and four small ones" regularity. Thus this match proves PWM frequency, duty as well as duration is configured properly. Moreover, peak-peak differences among sample values are huge enough to ensure the robustness. In the similar way, Fig. 12 and Fig. 13 present the "four large ones and two small ones" regularity.

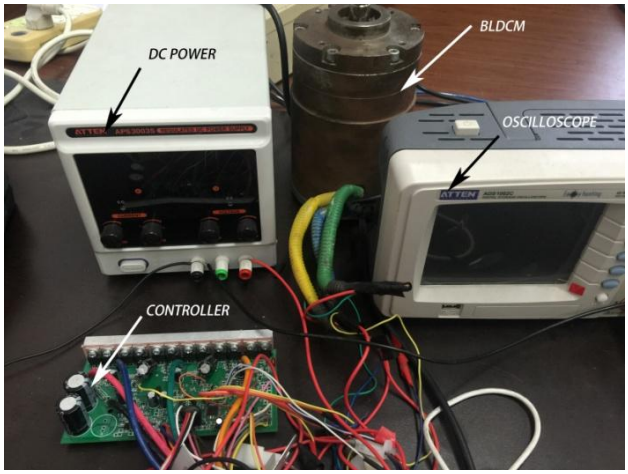

Fig. 9. The experimental setup

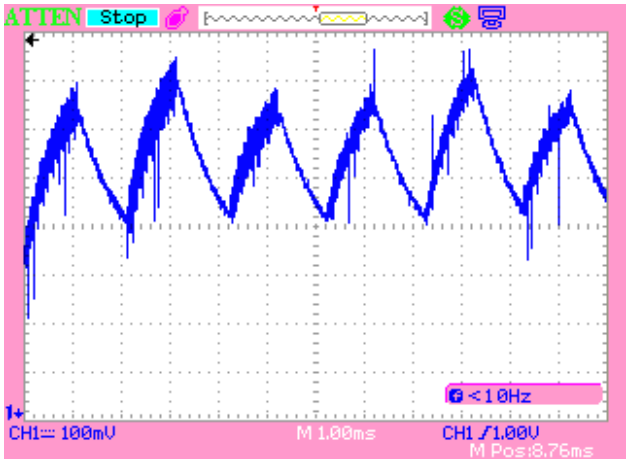

Fig. 10. "Two large ones and four small ones" regularity

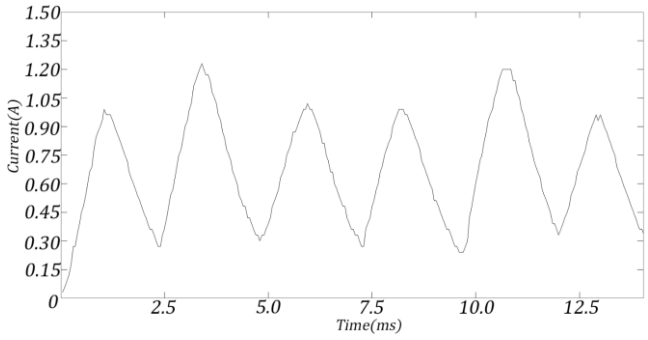

Fig. 11. Sampled "two large ones and four small ones" regularity

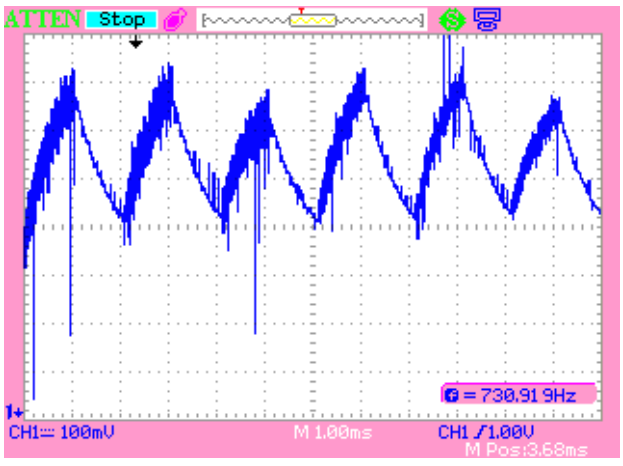

Fig. 12. "Four large ones and two small ones" regularity

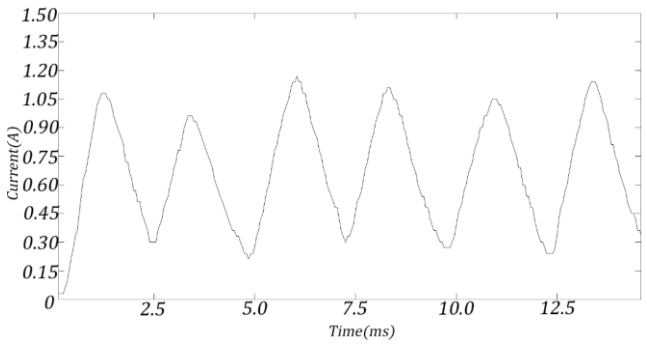

Fig. 13. Sampled "four large ones and two small ones" regularity

In the second estimation process, each opposite MMF lasts for 5ms with a 1-ms interval. The current value difference between the two opposite MMFs can be distinguished (as shown in Fig. 14).

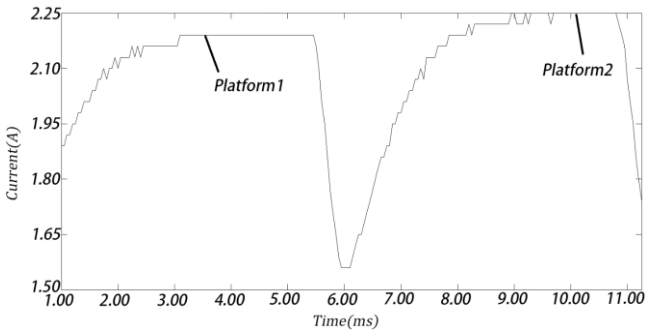

Fig. 14. Sampled current waveform of the two opposite MMFs in estimation process two

Fig. 15 depicts the starting current during the first 75ms since the machine starts. It's obvious that the machine under sensorless mode takes a rather long time to accelerate until the ZCP signal is caught for the purpose of stability. Before the commutation moment, the current rises slowly in ladder-like shape under a lower voltage on account of the limit of sampling precision. After catching the ZCP signal, the current surges to its peak and the motor starts a high-speed BEMF-based commutation mode.

However, current in hall-sensor-based mode rises sharply from the beginning, so the machine can enter the commutation stage immediately no matter how fast the rotor rotates. Hence, the first commutation in sensorless way comes later than that in hall-based way. Nevertheless, at the cost of starting torque and time, the sensorless way performs more flexibly.

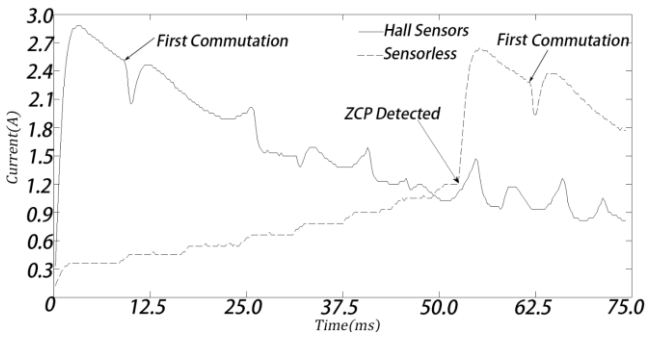

Fig. 15. Sampled current waveform of the starting period

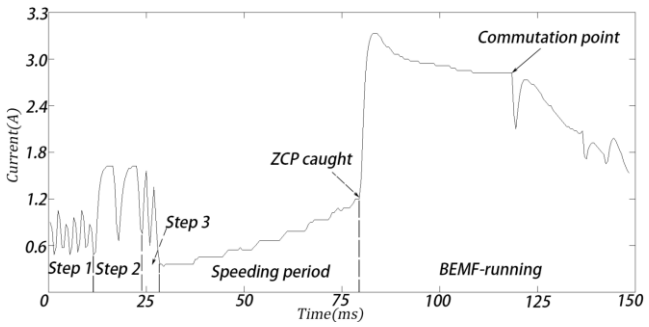

Fig. 16. Sampled current values during the whole starting procedure with no load

The engine starting period is expressed in Fig. 16 in which the starting period lasts for 80ms only. According to the current tendency, there is no reverse action in the whole sampling period and the rotor speeds up quickly ending up with entering the high-speed BEMF-based-running condition.

VI. Conclusion

Experiments have certified the feasibility of the starting method based on the high-precision estimation of the rotor position. This method can identify the rotor position within a maximum error of ± 7.5 in electrical degrees. With this more accurate rotor position information followed up with a low-speed startup pattern, vibration is lessen and reversal is avoided. Through this approach, sensorless BLDCM starts steadily which is very important in industrial applications such as pumps.

References

[1]. Quang-Vinh Tran and Tae-Won Chun," Simple Starting-up Method of BLDC Sensorless Control System for Vehicle Fuel Pump," The 2010 International Power Electronics Conference, pp. 2244-2248, 2010.

[2]. Tae-Won Chun and Quang-Vinh Tran,"Sensorless Control of BLDC Motor Drive for an Automotive Fuel Pump Using a Hysteresis Comparator," IEEE Transactions on Power Electronics, vol. 29, no. 3, 2014.

[3]. Mei Ying and Pan Zaiping, "A Novel Starting Method of Sensorless BLDC Motors for Electric Vehicles," 2010 International Conference on Electrical and Control Engineering, pp. 3212-3215, 2010.

[4]. Ogasawara S and Akagi H. "An approach to position sensorless drive for brushless DC motors," IEEE Transactions on Industry Applications, vol. 27, no. 5, pp. 928-933, 1991.

[5]. SHI Tingna, WU Zhiyong, and ZHANG Qian, "Sensorless Control of BLDC Motors Based on Variation Behavior of Winding Inductances," Proceedings of the CSEE, vol.32, no. 27, pp. 45-51, 2012.

[6]. Wook-Jin Lee and Seung-Ki Sul." A New Starting Method of BLDC Motors Without Position Sensor," IEEE Transactions on Industry Applications, vol. 42, no. 6, pp. 1532-1538, 2006.

[7]. A. Tashakori and M. Ektesabi, "Inverter Switch Fault Diagnosis System for BLDC Motor Drives," Engineering Letters, vol. 22, no. 3, pp. 118-124, 2014.

[8]. A. Tashakori and M. Ektesabi, "Position Sensors Fault Tolerant Control System in BLDC Motors," Engineering Letters, vol. 22, no. 1, pp. 39-46, 2014.

[9]. Tang Ningping and Cui Bin, "A High Resolution Detecting Method for Rotor Zero Initial Position of Sensorless Brushless DC Motor," Transaction of China Electrotechnical Society, vol. 28, no. 10, pp. 90-96, 2013.

[10]. Ren Lei, Cui Ruihua, and Wang Zongpei, "Saturation Effect of PMSM Windings Inductance," Transaction of China Electrotechnical Society, vol. 15, no. 1, pp. 21-25, 2000.

[11]. Krishnan R. Permanent magnet synchronous and brushless DC motor drives. CRC Press/Taylor & Francis, 2010.